IEICE TRANS. COMMUN., VOL.E87–B, NO.6 JUNE 2004

PAPER

Unsupervised Land Cover Classification Using $H/\bar{\alpha}/TP$ Space Applied to POLSAR Image Analysis

Koji KIMURA[†], ***Student Member***, **Yoshio YAMAGUCHI**[†], ***and*** **Hiroyoshi YAMADA**[†], ***Members***

SUMMARY This paper takes full advantage of polarimetric scattering parameters and total power to classify polarimetric SAR image data. The parameters employed here are total power, polarimetric entropy, and averaged alpha angle (alphabar). Since these parameters are independent each other and represent all the scattering characteristics, they seem to be one of the best combinations to classify Polarimetric Synthetic Aperture Radar (POLSAR) images. Using unsupervised classification scheme with iterative Maximum Likelihood classifier, it is possible to decompose multi-look averaged coherency matrix with complex Wishart distribution effectively. The classification results are shown using Pi-SAR image data set comparing with other representative methods.

key words: *total power, anisotropy, polarimetric entropy, alphabar, Wishart distribution, iterative ML method*

1. Introduction

The purpose of POLSAR image analysis is to classify land cover as accurate as possible using polarimetric scattering and intensity information. Since high resolution POLSAR data sets acquired with fully polarimetric airborne systems such as AIRSAR [1], Pi-SAR [2], and ESAR [3], are open to public, it is necessary to provide appropriate POLSAR image analysis tools.

There are many investigations on target decomposition based on covariance and coherency matrix, and on their applications to POLSAR image classification [4]–[9]. These decomposition methods rely on polarimetric scattering parameters and eigenvalues in the presence of speckle noise.

Among many decomposition schemes, the $H/\bar{\alpha}/$ anisotropy (A) method has been successfully proposed by Cloude, Pottier, and Lee [4]–[8] based on eigenvalues and eigenvectors of coherency matrix. The coherency matrix formulation has the advantages over covariance matrix method of relating to physical scattering mechanisms such as surface, multiple, dipole, and vegetation scattering, etc. Polarimetric entropy H shows randomness of a scattering medium, and alphabar $\bar{\alpha}$ represents average scattering mechanism. These two parameters are derived by decomposition of 3×3 coherency matrix [4]–[8]. Anisotropy ($A = \frac{\lambda_2 - \lambda_3}{\lambda_2 + \lambda_3}$) is introduced to classify targets effectively by the two minor eigenvalues [5], [6]. This method performs quite well in the case $\lambda_1 > \lambda_2 > \lambda_3$, where λ_i is an eigenvalue of coherency matrix. The eigenvalues are mathematically derived and physically correspond to scattering process [4]–[8]. However, it may cause classification errors in the case $\lambda_1 > \lambda_2 \approx \lambda_3$ ($A \approx 0$). This happens to regions where multiple scattering process occurs simultaneously. These areas physically correspond to vegetation areas, farm lands, and even some oriented urban areas with respect to SAR flight path [4], [5]. It is quite difficult to classify these areas or mixture of these areas accurately because these areas usually exhibit small Radar Cross Section (RCS), low anisotropy, and sometimes with high entropy.

In this paper, the authors propose alternatively the entropy (H)/alphabar ($\bar{\alpha}$)/total power (TP) method for such regions with low anisotropy and small RCS. In this method, A is replaced by total power TP. TP represents RCS of target (intensity information). This intensity information is important because it will serve to distinguish targets, for example, vegetation area and complex urban area where similar complex scattering process occurs simultaneously. Since it is one of the essential radar parameters, we use it for land cover classification. In addition, TP can simply be obtained by the sum of eigenvalues of coherency matrix, and is equivalent to the sum of square of scattering matrix elements.

The classification technique in this paper consists of unsupervised classification scheme using the $H/\bar{\alpha}/TP$ space and iterative Maximum Likelihood (ML) classifier based on the complex Wishart distribution [8], [9] for coherency matrix. The $H/\bar{\alpha}/TP$ space classifies POLSAR image into several clusters and provides feature coherency matrices for those clusters, which become training sets for initialization. Then, the image is iteratively classified by the ML classification method until a termination criterion is met. As preprocessing for land cover classification, polarimetric calibration [10], [11] is applied to POLSAR data. The data employed here is the L-band Pi-SAR data of the western part in Niigata City.

Section 2 introduces a brief principle of H, $\bar{\alpha}$, and TP, and a representation of the $H/\bar{\alpha}/TP$ space. Section 3 describes the unsupervised classification scheme. Sections 4 and 5 show the classification results comparing with other representative methods.

2. $H/\bar{\alpha}/TP$ Space

Polarimetric radar measures scattering matrix with quad-polarization. The scattering matrix in the hv polarization basis can be expressed as

$$[S(hv)] = \begin{bmatrix} S_{hh} & S_{hv} \\ S_{vh} & S_{vv} \end{bmatrix}. \quad (1)$$

Manuscript received August 7, 2003.
Manuscript revised November 6, 2003.

[†]The authors are with Niigata University, Niigata-shi, 950-2181 Japan.

For the reciprocal backscattering case, $S_{hv} = S_{vh}$. The coherency vector $\boldsymbol{k}_i$ based on the scattering matrix elements for ith pixel is defined by Eq. (2). The vector represents polarimetric scattering information [4]–[8]:

$$\boldsymbol{k}_i = \frac{1}{\sqrt{2}} \begin{bmatrix} S_{hh} + S_{vv} \\ S_{hh} - S_{vv} \\ 2S_{hv} \end{bmatrix}. \tag{2}$$

A one-look coherency matrix, T_i, of the ith pixel, is formed by the coherency vector $\boldsymbol{k}_i$,

$$T_i = \boldsymbol{k}_i \boldsymbol{k}_i^{\dagger}, \tag{3}$$

where the superscript † denotes complex conjugate transpose. The multi-look averaged coherency matrix, $\langle T \rangle$, is obtained by averaging n neighboring pixels,

$$\langle T \rangle = \frac{1}{n} \sum_{i=1}^{n} T_i. \tag{4}$$

This averaged matrix is a 3×3 Hermitian matrix and can be decomposed into

$$\langle T \rangle = \sum_{i=1}^{3} \lambda_i \boldsymbol{e}_i \boldsymbol{e}_i^{\dagger}, \tag{5}$$

where λ_i denotes an eigenvalue of the coherency matrix. These three eigenvalues are mathematically derived and their physical correspondence is scattering process [4]–[8]. $\boldsymbol{e}_i$ is an eigenvector represented as

$$\boldsymbol{e}_i = e^{j\phi_i} [\cos\alpha_i, \sin\alpha_i \cos\beta_i e^{j\delta_i}, \sin\alpha_i \sin\beta_i e^{j\gamma_i}]^t \quad (i = 1, 2, 3), \tag{6}$$

where the superscript t denotes matrix transpose. α_i represents a type of scattering mechanism. β_i denotes twice of polarization orientation angle [4], [5], [7]. The other parameters are summarized as follows [4], [5], [7]:

- ϕ_i: the phase of decomposed $hh + vv$ term,
- δ_i: the phase difference between decomposed $hh + vv$ and $hh - vv$ term,
- γ_i: the phase difference between decomposed $hh + vv$ and hv term.

Polarimetric entropy H, alphabar $\bar{\alpha}$, and total power TP can be obtained by eigenvalues and eigenvectors of the coherency matrix,

$$H = -\sum_{i=1}^{3} P_i \log_3 P_i, \; P_i = \frac{\lambda_i}{\sum_{j=1}^{3} \lambda_j} \; (i = 1, 2, 3), \tag{7}$$

$$\bar{\alpha} = \sum_{i=1}^{3} P_i \alpha_i, \tag{8}$$

$$TP = \sum_{i=1}^{3} \lambda_i = |S_{hh}|^2 + 2|S_{hv}|^2 + |S_{vv}|^2. \tag{9}$$

Polarimetric entropy H shows randomness of a scattering medium, and alphabar $\bar{\alpha}$ represents average scattering mechanism. Total power TP corresponds to RCS of target, which is equivalent to the sum of square of scattering matrix elements as represented by Eq. (9).

Anisotropy A, providing complement to H and facilitating scattering interpretation, can be derived by two minor eigenvalues λ_2 and λ_3 [5], [6] as follows:

$$A = \frac{\lambda_2 - \lambda_3}{\lambda_2 + \lambda_3}. \tag{10}$$

This parameter A becomes 0 for deterministic scatterer with $H = 0$ and for pure noise scatterer with $H = 1$. A high A indicates the presence of two scattering mechanisms, while a low A means the presence of a single dominant scattering mechanism or random scattering process. The low A regime is the most difficult area for classification. Figure 1 illustrates the H-$\bar{\alpha}$ plane [5], [7], [8]. Figure 2 shows the $H/\bar{\alpha}/A$ [5], [6], and the $H/\bar{\alpha}/TP$ space for which we propose in this paper.

The H-$\bar{\alpha}$ plane can represent all random scattering mechanisms. The physical scattering characteristics of the nine zones, Z1-Z9, shown in Fig. 1, are summarized as follows [5], [7], [8]:

Z1: High entropy multiple scattering,
Z2: High entropy vegetation scattering,
Z3: High entropy surface scatter,
Z4: Medium entropy multiple scattering,
Z5: Medium entropy vegetation scattering,
Z6: Medium entropy surface scatter,
Z7: Low entropy multiple scattering events,

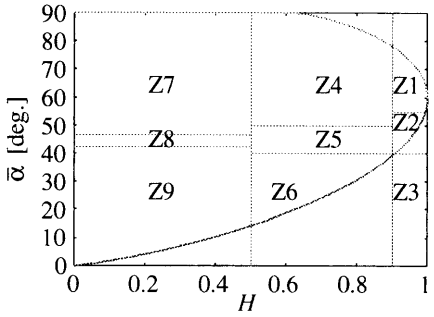

Fig. 1 H-$\bar{\alpha}$ plane.

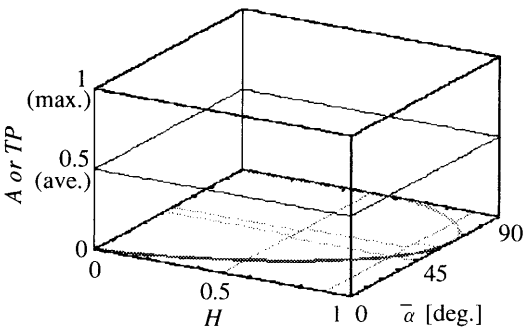

Fig. 2 $H/\bar{\alpha}/A$ or TP space.

Z8: Low entropy dipole scattering,
Z9: Low entropy surface scatter.

Z3 is not a feasible region in the H-$\bar{\alpha}$ plane. However, H is not a unique parameter for randomness of scatterer, because some combinations of the minor eigenvalues λ_2 and λ_3 yield the same H. Therefore, it happens that several different cluster centers locate in the same H-$\bar{\alpha}$ zone, which is not helpful for accurate classification.

The $H/\bar{\alpha}/A$ space compensates for the drawback of H-$\bar{\alpha}$ plane. The ability to distinguish classes is improved using this 3-dimensional space [5], [6]. The use of the space (addition of A) yields good land cover classification results in the case $\lambda_1 > \lambda_2 > \lambda_3$. However, it is expected that this method does not perform well in the regions such as forests, sparse urban area, and crop fields, etc., where $\lambda_1 > \lambda_2 \approx \lambda_3$ [4], [5], because several scattering mechanisms occur simultaneously, i.e., random volume scattering from canopy, surface scattering from several points, first order multiple scattering due to dielectric corner reflector, single scattering from isolated target. In these regions, A becomes less than 0.5, and H is relatively high. A causes classification errors due to similar scattering process.

The $H/\bar{\alpha}/TP$ space will compensate for both the drawbacks of H-$\bar{\alpha}$ plane and $H/\bar{\alpha}/A$ space for these regions. The total power has three merits:

I) The parameter is insensitive to noise, compared to A,
II) The value provides us with information on the magnitude of scatterer, i.e., RCS. It is independent of polarization basis, and therefore is polarization invariant quantity.
III) The parameter is independent of H, $\bar{\alpha}$, and A. It provides complement to H and facilitates interpretation of terrain types.

The combination of $H/\bar{\alpha}/TP$ will be effective in discrimination of vegetation and residential area where similar complex scattering process occurs simultaneously. The discrimination of these two areas is one of the most important and difficult subjects in land cover classification.

3. Unsupervised Classification Scheme

The unsupervised land cover classification scheme in this paper is based on polarimetric scattering and intensity parameters (H, $\bar{\alpha}$, and TP) and iterative Maximum Likelihood (ML) classifier. Fortunately, H, $\bar{\alpha}$, and TP can be easily obtained by multi-look averaged coherency matrix (4). First, the classification forms initial cluster centers V_i of coherency matrices, which are represented as follows:

$$V_i = \frac{1}{n_i} \sum_{j=1}^{n_i} \langle T \rangle_j , \tag{11}$$

where n_i is the number of pixels belonging to class i. They become training sets for iterative ML classifier. Also, each cluster center provides its polarimetric scattering and intensity information (the values of H, $\bar{\alpha}$, and TP).

The ML classification is based on the complex Wishart distribution [8], [9] for averaged coherency matrix. A distance measure between $\langle T \rangle$ and the cluster center V_m, of class m is represented by the following equation.

$$d(\langle T \rangle, V_m) = n[\ln |V_m| + \mathrm{Tr}(V_m^{-1} \langle T \rangle)] - \ln[P(m)], \tag{12}$$

where $P(m)$ is a priori probability of class m, and n is the number of looks. Tr denotes the trace of a matrix. Without knowledge of the probability, $P(m)$ is assumed to be equal for all m, and therefore an equivalent distance measure becomes

$$d(\langle T \rangle, V_m) = \ln |V_m| + \mathrm{Tr}(V_m^{-1} \langle T \rangle). \tag{13}$$

This distance measure can be applied to multi-look processed POLSAR data since it is independent of the number of looks [8], [9]. A pixel in POLSAR image is assigned to a class with the minimum distance. The pixel is assigned to class m, if

$$d(\langle T \rangle, V_m) \leq d(\langle T \rangle, V_j) \quad \text{for all } j \neq m. \tag{14}$$

In the iterative ML classification, the classified image is used to update all the existent cluster centers. The updated centers become new training sets for classification in the next iteration, on the basis of (11), (13), and (14). This process is repeated until a termination criterion is met. The termination criterions are predetermined by number of iterations, number of pixels switching classes, and the maximum separation between classes. In this paper, the number of iterations is 15. In this case, the ratio of pixels switching classes is smaller than 5%.

4. Unsupervised Classification Results

The authors analyzed the L-band Pi-SAR image data set provided by CRL/NASDA, which is an image of the western part in Niigata City, Japan. The scene contains Niigata university, residential area, the Sea of Japan, river (the Shinkawa River), crop fields, paddy fields, and pine woods. Figures 3 and 4 show the site map, and photo around university (which can be ground truth data), respectively. The details of data set are listed in Table 1. As preprocessing

Fig. 3 The map of the western part in Niigata City.

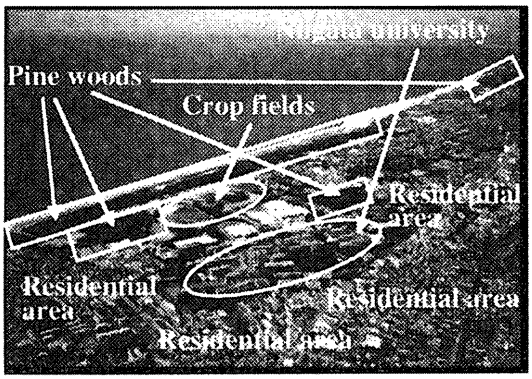

Fig. 4 Photo around Niigata university.

Table 1 The L-band Pi-SAR data characteristics for the western part in Niigata City.

Frequency	1.27 GHz
Data-take	13 June, 2002
Polarization	HH, HV, VH, VV
Incidence Angle	29.5-43.4 deg.
Image Size	4 by 4 km
Dimension	1600 by 1600 pixels

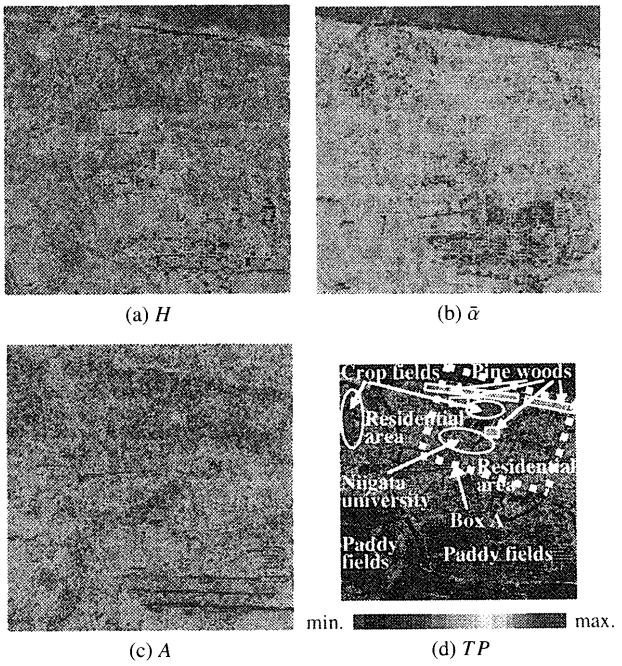

(a) H (b) $\bar{\alpha}$ (c) A (d) TP

Fig. 5 Entropy, alphabar, anisotropy, and total power images of the western part in Niigata City: (a) entropy, (b) alphabar, (c) anisotropy, and (d) total power.

for classification, polarimetric calibration [10], [11] is carried out using a 7 by 7 pixel window on the Pi-SAR data.

Figure 5 illustrates the entropy, alphabar, anisotropy, and total power images for the site. Box A shown in Fig. 5(d) corresponds to the region illustrated in Fig. 4. It can be seen in Fig. 5 that the difference of polarimetric scattering characteristics do not appear so clearly, especially

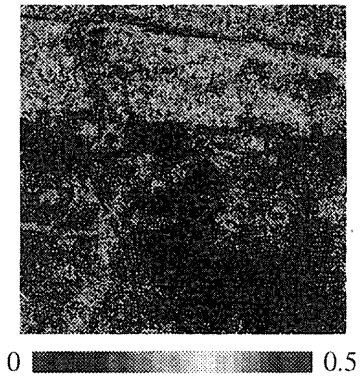

black area: $A \geq 0.5$.
(a) A

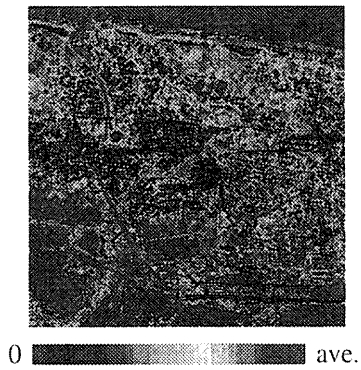

black area: $TP \geq ave.$
(b) TP

Fig. 6 Anisotropy (less than 0.5), and total power (smaller than average) images of the western part in Niigata City: (a) anisotropy, and (b) total power.

around the university. The dynamic ranges of H and $\bar{\alpha}$ are narrow. The value of $\bar{\alpha}$ is approximately 45° and is uniformly distributed throughout the image except for the Sea of Japan, part of residential area and paddy fields. In this POLSAR data, several target areas, such as pine woods, crop fields, residential area around university exhibit similar polarimetric scattering characteristics with high H, moderate $\bar{\alpha}$ (40° – 50°), and A less than 0.5. Therefore, it is difficult to distinguish targets using polarimetric scattering parameters H, $\bar{\alpha}$ and A only for this scene.

Figure 6 shows the regions with A less than 0.5, and TP smaller than the entire average. The purpose is to see the land targets with anisotropy less than 0.5 and small RCS area. These regions are difficult to be classified. The regions with A larger than 0.5 and TP greater than the average are colored black in this figure. The difference of TP (RCS) appears clearly in Fig. 6(b) compared to that of A in Fig. 6(a). In addition, it is seen in Fig. 6(b) that A is noisy. Therefore, it is expected that TP may serve efficiently to classification for these regions.

The land cover classification results for the site based on H-$\bar{\alpha}$ plane, $H/\bar{\alpha}/A$ and $H/\bar{\alpha}/TP$ spaces, and their comparison are shown in the next section.

5. Comparison of $H/\bar{\alpha}/A$ and $H/\bar{\alpha}/TP$

In the case of classification based on the H-$\bar{\alpha}$ plane, the maximum number of classes is 8 according to feasible zones in Fig. 1. For the $H/\bar{\alpha}/A$ space, the number is 16, because 8 feasible zones in the H-$\bar{\alpha}$ plane are divided into two classes: one with A larger than 0.5, and another with A less than 0.5. As for the $H/\bar{\alpha}/TP$ space, 16 classes are set up in a similar way to the $H/\bar{\alpha}/A$ space (see Fig. 2). The division is made by TP value being larger or less than criterion value. As the criterion value, the average TP for all the pixels in the image is simply used. The class i ($1 \leq i \leq 8$) for the H-$\bar{\alpha}$ plane is divided into class $2i-1$ and class $2i$, for the $H/\bar{\alpha}/A$ and $H/\bar{\alpha}/TP$ spaces.

Figure 7 illustrates classified images, based on the H-$\bar{\alpha}$ plane, $H/\bar{\alpha}/A$ and $H/\bar{\alpha}/TP$ spaces. Final cluster centers of each class, and initial color codes for each H-$\bar{\alpha}$ zone are shown in Fig. 8. Each color used for classified images in Fig. 7 is labeled with corresponding number shown in initial color code distribution, and final cluster centers in Fig. 8. In addition, the values of H, $\bar{\alpha}$ and A or TP for each cluster center in Figs. 8(b), (e), and (h) are listed in Table 2.

With respect to classification based on the H-$\bar{\alpha}$ plane, it can be seen in Fig. 7(a) that a lot of land targets cannot be distinguished due to similarity of scattering mechanisms. For example, pine woods and residential areas around university are assigned to the same class. Similarly, the Sea of Japan and paddy fields cannot be discriminated. The several final cluster centers locate in the same H-$\bar{\alpha}$ zone, Z5 and Z9 (see Fig. 8(b)). These results mean that the H-$\bar{\alpha}$ plane is not sufficient to distinguish targets and to identify the types of terrain.

As seen in Fig. 7(b), there still exist classification errors in several target areas, although the sea and paddy fields can be discriminated well by supplemental information of A. The discrimination among crop fields, pine woods and residential areas around university is not well done due to similarity of polarimetric scattering characteristics. In addition, the several final cluster centers still concentrate in Z5 because of similar scattering process as shown in Fig. 8(e).

In contrast, $H/\bar{\alpha}/TP$ space yields rather good classification results. The enlargement of the classification results for region A shown in Figs. 7(b) and (c), and some photos are illustrated in Fig. 9 for the comparison. The authors picked up three areas A-C as shown in this figure:

Area A: Mixture of crop fields and some buildings,
Area B: Mixture of pine woods area and some houses,
Area C: Crop field.

$H/\bar{\alpha}/TP$ method can discriminate buildings and houses from crop fields and pine woods area in the small rectangular boxes A-B. In addition, classification errors do not occur in box C. The pine woods area, crop fields, and buildings and houses are colored dark green, light green, and red in these boxes in Fig. 9(a), respectively. However, $H/\bar{\alpha}/A$ method cannot fully discriminate buildings and houses from crop fields and pine woods area in boxes A-B (see Fig. 9(b)).

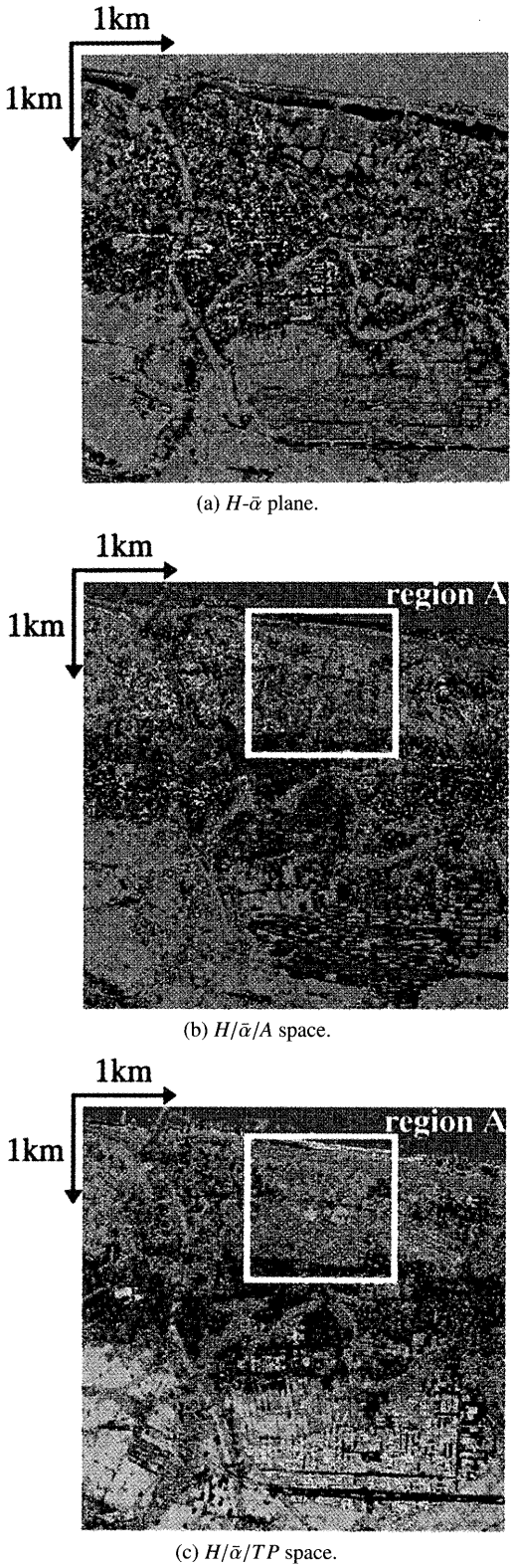

(a) H-$\bar{\alpha}$ plane.

(b) $H/\bar{\alpha}/A$ space.

(c) $H/\bar{\alpha}/TP$ space.

Fig. 7 Classification results of the western part in Niigata City.

The classification errors occur in dark green area within box C. In addition, it is seen in Fig. 9 that A is noisy. For the $H/\bar{\alpha}/TP$ space, paddy fields are also assigned to several classes because of the presence of canopy, surface roughness, and soil moisture (see Fig. 7(c)). Moreover, several

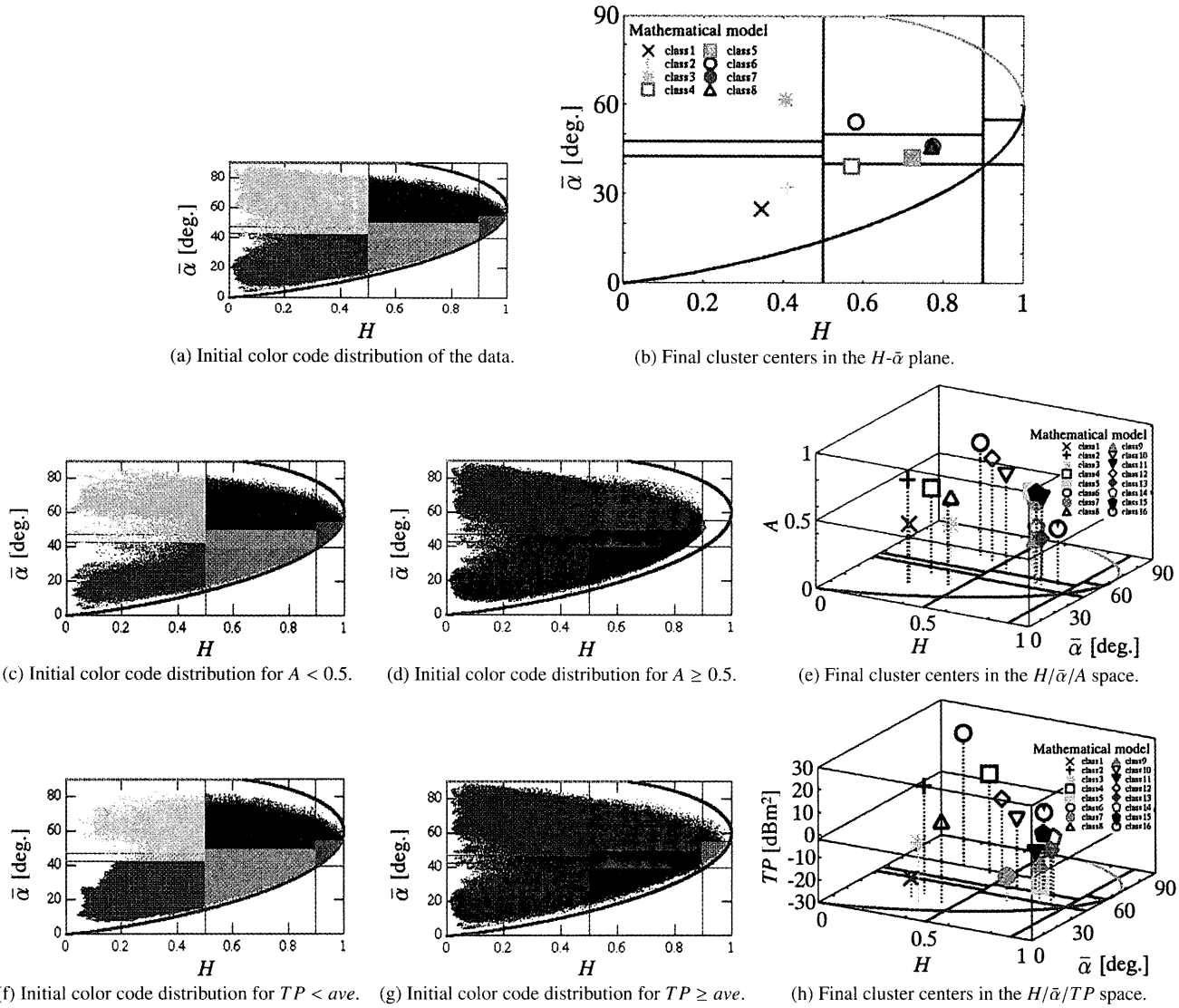

(a) Initial color code distribution of the data.
(b) Final cluster centers in the H-$\bar{\alpha}$ plane.
(c) Initial color code distribution for $A < 0.5$.
(d) Initial color code distribution for $A \geq 0.5$.
(e) Final cluster centers in the $H/\bar{\alpha}/A$ space.
(f) Initial color code distribution for $TP < ave.$
(g) Initial color code distribution for $TP \geq ave.$
(h) Final cluster centers in the $H/\bar{\alpha}/TP$ space.

Fig. 8 Initial color code distribution, and final cluster centers for the western part in Niigata City.

footpaths between rice paddies are discriminated from the paddy fields. As illustrated in Fig. 8(h), the final cluster centers in Z5 are spread compared to Fig. 8(e). The classification results show that $H/\bar{\alpha}/TP$ space is effective for discriminating vegetation and residential area, where the polarimetric scattering property is characterized with A less than 0.5 and relatively high H.

In Figs. 7 and 8, the full dynamic range of TP is used for classification. It is expected that the ability to distinguish targets may be further improved as the number of dynamic range division increases. The dynamic range division is deeply related to terrain type and distribution in SAR data, and way of stochastic subdivision with respect to TP. Therefore, the effects of these factors in land cover classification should be considered.

SAR image data have very large dynamic range (for example, 50 dBm^2) specific to acquired scene. Therefore, the best number of TP division depends on the scene. In this example, the authors tried to divide TP range into 2, 4, 6, and 8 classes. Figure 10 illustrates the classification results according to (a) 4-class division; (b) 6-class division; and (c) 8-class division, which correspond to 32, 48, and 64 classes, respectively. Note that each color used for these figures does not correspond to class number shown in Figs. 7 and 8.

Figure 10 shows that the 2-class division classification has performed the best in this specific scene. Assignment errors to residential class in pine woods area along the coastline are reduced in the 4-class division case. More roads and footpaths are discriminated well from other targets for the 6-, and 8-class division. However, classification errors increase in crop fields and pine woods areas around university for the 4-, 6-, and 8-class division cases.

Effective methods of class subdivision with respect to TP should be investigated in the future.

6. Conclusion

Unsupervised land cover classification using polarimetric entropy H, alphabar $\bar{\alpha}$, and total power TP was proposed

Table 2 The lists of each cluster center.

(a) H-$\bar{\alpha}$ plane.

Class	H	$\bar{\alpha}$ [deg.]
1	0.346	24.97
2	0.411	32.45
3	0.406	61.69
4	0.571	39.20
5	0.722	42.41
6	0.582	54.17
7	0.774	46.15
8	0.771	45.51

(b) $H/\bar{\alpha}/A$ space.

Class	H	$\bar{\alpha}$ [deg.]	A	Class	H	$\bar{\alpha}$ [deg.]	A
1	0.287	23.42	0.429	**9**	0.763	40.67	0.351
2	0.287	22.59	0.760	**10**	0.551	53.49	0.708
3	0.465	29.54	0.441	**11**	0.722	52.73	0.590
4	0.287	39.72	0.605	**12**	0.490	52.68	0.811
5	0.635	58.75	0.576	**13**	0.777	43.41	0.353
6	0.378	61.33	0.843	**14**	0.757	43.17	0.435
7	0.719	49.10	0.578	**15**	0.685	54.62	0.608
8	0.461	27.17	0.646	**16**	0.819	49.26	0.406

(c) $H/\bar{\alpha}/TP$ space.

Class	H	$\bar{\alpha}$ [deg.]	TP [dBm^2]	Class	H	$\bar{\alpha}$ [deg.]	TP [dBm^2]
1	0.286	23.39	-21.98	**9**	0.772	41.08	-13.29
2	0.321	27.41	18.06	**10**	0.608	50.51	1.00
3	0.322	22.90	-5.53	**11**	0.674	53.45	-13.47
4	0.430	58.23	15.10	**12**	0.495	57.21	5.49
5	0.719	50.02	-26.77	**13**	0.801	44.98	-7.93
6	0.283	62.17	29.40	**14**	0.803	46.32	-2.37
7	0.652	36.40	-19.19	**15**	0.714	53.02	-4.39
8	0.421	24.47	4.68	**16**	0.705	55.06	3.87

for POLSAR image analysis. These polarimetric scattering and intensity parameters are derived directly by eigenvalues and eigenvectors of multi-look averaged coherency matrix. This method will serve to classify land targets including distributed natural and man-made targets with anisotropy A less than 0.5, and relatively high entropy H, such as crop field, forest and residential area, etc. The comparison with other representative classification results using Pi-SAR data set shows that $H/\bar{\alpha}/TP$ space is effective for distinguishing between vegetation and residential area.

Acknowledgments

The authors would like to thank CRL/NASDA for providing valuable Pi-SAR image data sets. This work in part was supported by Grant in Aid for Scientific Research, JSPS, Japan.

References

[1] http://airsar.jpl.nasa.gov
[2] http://www2.crl.go.jp/dk/c215/index.html
[3] http://www2.dlr.de/NE-HF/projects/ESAR
[4] S.R. Cloude and E. Pottier, "A review of target decomposition theorems in radar polarimetry," IEEE Trans. Geosci. Remote Sens., vol.34, no.2, pp.498–518, March 1996.
[5] S.R. Cloude, I. Hajnsek, and K.P. Papathanassiou, "An eigenvector method for the extraction of surface parameters in polarimetric SAR," Proc. CEOS SAR Workshop, Toulouse, France, ESA SP-450, March 2000.
[6] E. Pottier and J.S. Lee, "Application of the $\langle\langle H/\bar{\alpha}/TP\rangle\rangle$ polarimetric decomposition theorem for unsupervised classification of fully polarimetric SAR data based on the Wishart distribution," Proc. Committee on Earth Observing Satellites SAR workshop, CNES, Toulouse, France, Oct. 1999.
[7] S.R. Cloude and E. Pottier, "An entropy based classification scheme for land applications of polarimetric SAR," IEEE Trans. Geosci. Remote Sens., vol.35, no.1, pp.68–78, Jan. 1997.
[8] J. Lee, M.R. Grunes, T.L. Ainsworth, L. Du, D.L. Schuler, and S.R. Cloude, "Unsupervised classification using polarimetric decomposition and the complex Wishart classifier," IEEE Trans. Geosci. Remote Sens., vol.37, no.5, pp.2249–2258, Sept. 1999.
[9] J.S. Lee, M.R. Grunes, and R. Kwok, "Classification of multi-look polarimetric SAR imagery based on complex Wishart distribution," Int. J. Remote Sensing, vol.15, no.11, pp.2299–2311, 1994.
[10] J.J. van Zyl et al., "Calibration of polarimetric radar images using only image parameters and trihedral corner reflector responses," IEEE Trans. Geosci. Remote Sens., vol.28, no.3, pp.337–348, May 1990.
[11] R.A. Cordey, "On the accuracy of crosstalk calibration of polarimetric SAR using natural clutter statistics," IEEE Trans. Geosci. Remote Sens., vol.31, no.2, pp.447–454, March 1993.

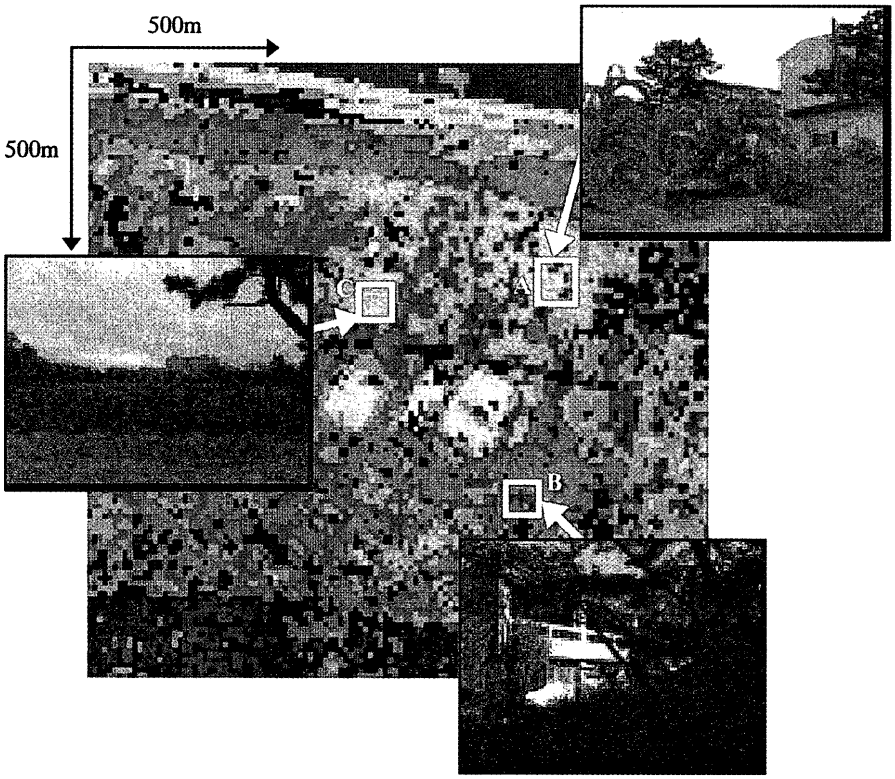

(a) $H/\bar{\alpha}/TP$ space.

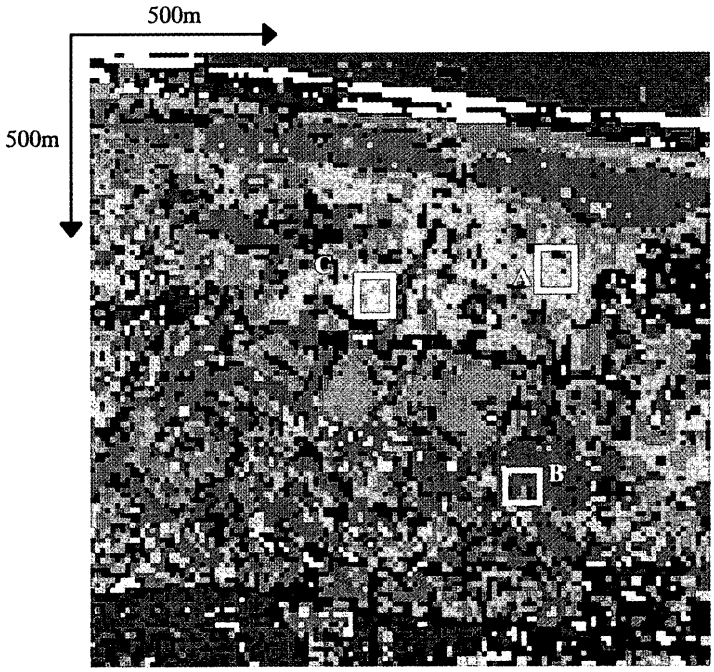

(b) $H/\bar{\alpha}/A$ space.

Fig. 9 The comparison of ground truth and classification results around Niigata university.

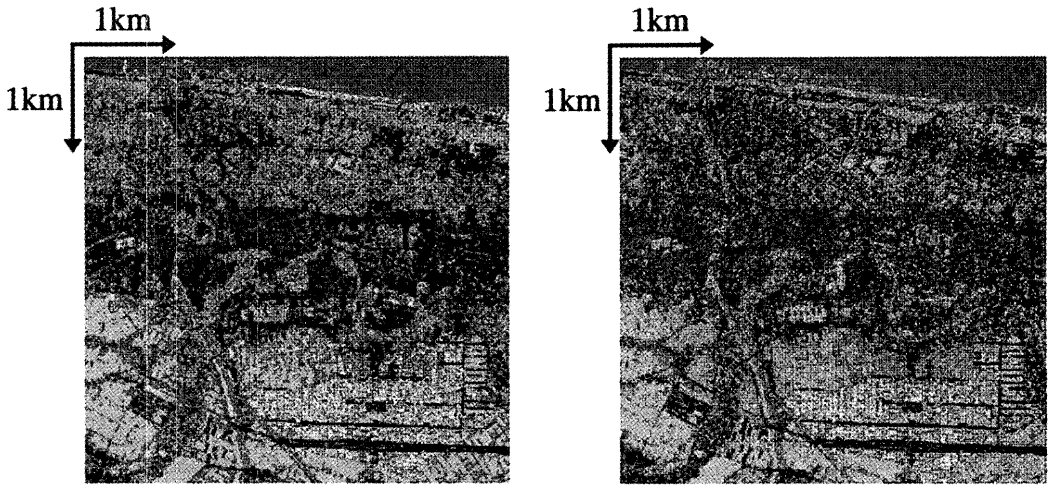

(a) 4-class division. (b) 6-class division.

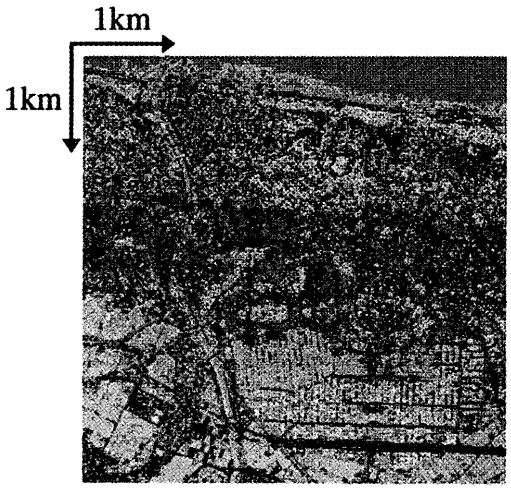

(c) 8-class division.

Fig. 10 Variation of classification results of the western part in Niigata City in the case of class subdivision with respect to TP.

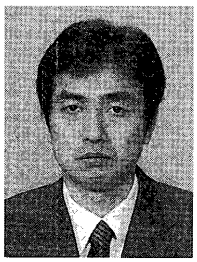

Koji Kimura was born in Niigata, Japan, on March 1, 1976. He received the B.E. and M.E. degrees from Niigata University, Niigata, Japan, in 1998 and 2000, respectively. He is currently working toward the Ph.D. degree in information engineering at the same University. He is now engaged in SAR image analysis and target classification using radar polarimetry.

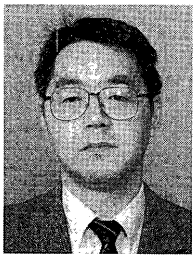

Yoshio Yamaguchi received the B.E. degree in electronics engineering from Niigata University in 1976, and the M.E. and Dr. Eng. degrees from Tokyo Institute Technology in 1978 and 1983, respectively. In 1988, he joined the Faculty of Engineering, Niigata University, where he is a professor. From 1988 to 1989, he was a Research Associate at the University of Illinois, Chicago. His interests are in the field of propagation characteristics of electromagnetic waves in lossy medium, radar polarimetry, microwave remote sensing and imaging. Dr. Yamaguchi is a Fellow of IEEE, and a member of the Japan Society for Snow Engineering.

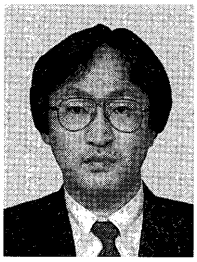

Hiroyoshi Yamada received the B.E., M.E., and Dr. Eng. degrees from Hokkaido University, Sapporo, Japan, in 1988, 1990 and 1993, respectively, all in electronic engineering. In 1993, he joined the Faculty of Engineering, Niigata University, where he is an associate professor. From 2000 to 2001, he was a Visiting Scientist at Jet Propulsion Laboratory, California Institute of Technology, Pasadena. His current interests involve in the field of array signal processing, radar polarimetry and interferometry, microwave remote sensing and imaging. Dr. Yamada is a member of IEEE.